# Strategies for Control of the Space Shuttle Transition

ROBERT F. STENGEL*
*Charles Stark Draper Laboratory, MIT*
*Cambridge, Mass.*

**The space shuttle will re-enter the Earth's atmosphere at high angle of attack, in order to minimize total heat load, and will perform a transition to low angle of attack for increased trajectory control. The timing and shaping of this angle transition are affected by specific-control-moment boundaries, attitude instability, angle of attack, limits on various flight parameters, and the establishment of a trimmed condition for flight to the landing site. Transitions to altitudes between 45,000 and 150,000 ft are investigated here, with particular attention given to suitable terminal conditions and to stability and control boundaries. Angle of attack is the control variable; hence, the short-period dynamics are not modeled. Two degree-of-freedom trajectories are optimized using a steepest descent algorithm with automatic step-sizing and open end-time. It is found that trim-glide flight-path angle $\gamma$ becomes very steep as altitude increases and that trajectories to such flight conditions are difficult to achieve. High-altitude equilibrium conditions ($\dot{\gamma} = 0$) at zero $\gamma$ are readily obtained, and they provide suitable way points for a continued glide to low altitude. Dynamic pressure and load factor peaks associated with both types of transition are not excessive. Stability and control boundaries have significant effects on the trajectories, although peak load, dynamic pressure and load factor are not materially altered. Gliding trajectories from high to low altitude are found to be sensitive to phugoid mode excitation, and the dynamic pressure peak which occurs prior to the terminal flight condition may be excessive.**

## Introduction

THE success of the space shuttle program depends, in large part, upon the orbiter's ability to return a substantial payload from orbit, to maneuver to landing sites which lie a moderate distance from the ground track of the initial orbital plane, and to perform a conventional aircraft landing. The dominant constraint on the return phase of the space shuttle mission is aerodynamic heat load, for this determines the extent (and weight) of heat shielding, and it imposes limitations on the trajectory. It is not surprising, then, that nominal mission profiles for the straight- and delta-wing configurations[1-3] coalesced on the high $\alpha$/low $\alpha$ trajectory first proposed by the staff of the NASA Langley Research Center in 1959.[4] In this concept the spacecraft begins entry at a high angle of attack $\alpha$ transitioning to low-$\alpha$ flight once the peak heating is passed. By flying at high angle of attack, heating is localized to the lower surface of the spacecraft, and the surface area requiring shielding against high temperatures is minimized. The rotation to low-$\alpha$ brings increased lift-drag ratio, with a concomitant improvement in trajectory control.

Previous studies of subsonic transition maneuvers for the straight-wing configuration have used optimal control theory to shape trajectories, subject to angle-of-attack and load factor penalties,[5] and have used these results to specify rotational control requirements.[6] The subsonic transition is complicated by a pitchup instability at angles intermediate to the entry angle (60°) and the subsonic cruise angle of attack (taken to be 4° in these reports). This work indicated that $\alpha$-profiles which jump the unstable region while meeting trim-glide flight conditions at the end can be found, and that proper choice of the jump duration allows the jump to be made with modest elevator control power, at pitch rates below 10°/sec, and without stability augmentation (although rate damping has a beneficial effect). These reports were premised on incomplete aerodynamic data (applicable only to low-subsonic and hypersonic Mach numbers), and terminal altitudes were restricted to 60,000 ft or less to assure subsonic equilibrium velocities. Elevator effectiveness was assumed to be linear and unlimited. Subsequent data provide a clearer look at the effects of Mach number and the moment due to control. As will be shown in a later section, these data indicate that the subsonic transition maneuver is more difficult than anticipated and that the limits of control authority can not be ignored.

This paper explores the subject of high altitude, supersonic transitions for the straight-wing orbiter, incorporating an improved description of Mach number and control effects. Histories of the control variable (angle of attack) and selected flight parameters from optimal trajectories are examined. Static pitch moment characteristics are used to define the allowable bounds of angle of attack (as a function of Mach number), and the variations in optimal trajectories which these limits cause are discussed. Pitching motions are not modeled, so it is assumed that the vehicle follows the desired $\alpha$-profile precisely. The trajectories for this study begin at a Mach number of 10.4 and an altitude of 180,000 ft, terminating at altitudes of 45,000–150,000 ft and Mach numbers of 0.87–8.1. The two degree-of-freedom trajectories are optimized using steepest descent and conjugate gradient algorithms with automatic step-sizing and open end-time.

## Description of Equations

The translational equations for a rigid, nonthrusting body moving about a nonrotating spherical Earth are

$$\dot{x}_1 = -D/m - g\cos x_2 \tag{1}$$

$$\dot{x}_2 = [g/x_1 - x_1/(R + x_3)]\sin x_2 - L/mx_1 \tag{2}$$

$$\dot{x}_3 = x_1\cos x_2 \tag{3}$$

$$\dot{x}_4 = x_1\sin x_2/(1 + x_3/R), \tag{4}$$

where the state variables (in order) are velocity magnitude, flight-path angle (from the vertical), altitude, and range along the Earth's surface. The gravitational acceleration $g$ is consistent with an inverse-square field, the mass $m$ is constant, and the lift and drag forces, $L$ and $D$, are functions of the state and the control variable, $\alpha$ (angle of attack).

The optimization uses the Euler-Lagrange equations for the adjoint variable $\bar{\lambda}$

$$\dot{\bar{\lambda}} = -\mathbf{f}_x{}^T\bar{\lambda} - \bar{\mathscr{L}}_x{}^T \tag{5}$$

Presented as Paper 71-921 at the AIAA Guidance Control and Flight Mechanics Conference, Hempstead, N.Y., August 16–18, 1971. This research was supported by NASA Contract NAS9-10268.

Index categories: Entry Vehicle Mission Studies and Flight Mechanics; Entry Vehicle Dynamics and Control; Spacecraft Navigation, Guidance and Flight-Path Control Systems.

* Group Leader. Member AIAA.

and the control perturbation $\delta\alpha$

$$\delta\alpha = -k(\mathscr{L}_\alpha + \bar{\lambda}^T \bar{f}_\alpha)^T \tag{6}$$

to minimize the cost function $J$[7]

$$J = \Phi(\bar{x} - \bar{x}_c) + \int_0^{t_f} \mathscr{L} dt \tag{7}$$

Here, $\Phi(\bar{x} - \bar{x}_c)$ is the quadratic cost of terminal state errors

$$\Phi(\bar{x} - \bar{x}_c) = (\bar{x} - \bar{x}_c)^T \mathbf{Q} (\bar{x} - \bar{x}_c) \tag{8}$$

The starting values for the backward integration of $\bar{\lambda}$ from the final time $t_f$ to the initial time (zero) are found by evaluating $\partial\Phi/\partial\bar{x}$ at $t = t$. $\mathbf{Q}$ is a diagonal weighting matrix whose coefficients establish acceptable tradeoffs between terminal state errors. The Lagrangian $\mathscr{L}$ of the integral cost in Eq. (7) consists of a quadratic penalty for load factors other than 1

$$\mathscr{L}_1 = k_1[(L^2 + D^2)^{1/2}/m - g]^2 \tag{9}$$

and an angle attack penalty function comprised of 2 parts. The first penalizes angles outside $\alpha_0$ and $\alpha_3$ and in the intermediate region, $(\alpha_1, \alpha_2)$

$$\mathscr{L}_{21} = \begin{cases} k_2(\alpha - \alpha_0)^2, & \alpha < \alpha_0 \\ 0, & \alpha_0 \le \alpha \le \alpha_1 \\ k_3 \sin^2\pi\left(\dfrac{\alpha - \alpha_1}{\alpha - \alpha_2}\right), & \alpha_1 < \alpha < \alpha_2 \\ 0, & \alpha_2 \le \alpha \le \alpha_3 \\ k_2(\alpha - \alpha_3)^2, & \alpha > \alpha_3 \end{cases} \tag{10}$$

where $\alpha_0$, $\alpha_1$, $\alpha_2$, and $\alpha_3$ are functions of the Mach number $M$.

The second $\alpha$-penalty is a time-varying soft constraint on initial and final angles, $\alpha_s$ and $\alpha_f$

$$\mathscr{L}_{22} = k_2\{(\alpha - \alpha_s)^2/(1 + t^3) + (\alpha - \alpha_f)^2/[1 + (t_f - t)^3]\} \tag{11}$$

Two algorithms, the steepest descent-[7] and the conjugate gradient methods,[8] have been used for numerical optimization in conjunction with a one-dimensional search. The steepest descent method uses Eq. (6) to form the control correction on each iteration; the conjugate gradient method blends previous control corrections into the current correction in an attempt to take a more direct path to the minimum of a quadratic cost function. Present experience with the conjugate gradient technique appears to confirm earlier findings,[9,10] i.e., that improved convergence is not reliably demonstrated in highly nonlinear problems.

The one-dimensional search finds a local minimum in $J$ with respect to the $k$ of Eq. (6) by computing test trajectories and fitting a quadratic curve to the 3 points identifying a tabulated minimum in $J$ (the minimum point and its immediate neighbors). The trajectory is recomputed with the control perturbed by Eq. (6), where $k$ is the minimizing value for the quadratic fit to $J$. Final time is adjusted by searching the costs in the vicinity of the nominal stop time for a tabulated minimum, then fitting a curve to this and the adjacent 2 points to obtain the quadratic minimum. The adjustment is made at the beginning of each iteration; thus, the step-size adjustment for each iteration is a fixed-time optimization.

## Application to Orbiter Transition

The numerical results which follow pertain to a preliminary orbiter design with a 15,000-lb payload capacity.[11] The craft's entry wing loading is 111 psf. Although the maximum hypersonic lift-drag ratio, $L/D$, is 1.4, the 60° entry angle of attack chosen to reduce aerodynamic heating yields an $L/D$ of 0.53. $L/D_{max}$ is 8.3 at $M = 0.3$.

After describing the initial and final conditions for the transition trajectories, the optimal flight paths connecting these end points are presented. The first group of trajectories have locally minimum load factor and are not subjected to angle constraints. The angle-of-attack boundaries imposed by stability-and-control characteristics are discussed in the following section. Constraining the transition trajectories to avoid uncontrollable regions and to jump through imbedded unstable regions is a means of reducing control requirements for the vehicle; flight paths which accomplish this are demonstrated. The concept of a two-stage transition from high- to low-$\alpha$ is introduced; the first $\alpha$-reduction occurs at high $M$ and is followed by a gliding trajectory to the high-key point which defines the start of the terminal area guidance phase. The existence of at least 2 locally minimizing paths is shown in the final section, which compares a maximum range trajectory to the previous results.

### Initial Condition

The starting point for this study has been determined by the heating constraint. Ninety-five percent of the aerodynamic heating during an entry at 50° bank angle (a high cross-range trajectory) has occurred by the time that the spacecraft reaches a 180,000-ft altitude and a Mach number of 10.4. The accumulated stagnation point heat load is 31,350 BTU/ft$^2$, with 1565 BTU/ft$^2$ of heating remaining (assuming that the flight continues at $\alpha = 60°$). Flight path angle, dynamic pressure, and load factor are $-1.8°$, 68 psf, and 2.41 $g$'s. This condition is taken as the starting point, with the further assumption that the vehicle has returned instantaneously to zero roll angle. Angle of attack is free to vary from this point on, subject to the constraints described in the previous section.

### Terminal Conditions

The terminal conditions lie in the entry plane and have a single common characteristic: given the proper $\alpha$ for $L/D_{max}$, the time-rate of change of the flight-path angle ($\gamma = \pi/2 - x_2$) is zero. The conditions are divided into 3 categories. In the first case, the terminal flight path angle, $\gamma$, also is zero, and the spacecraft is temporarily in horizontal flight; with air-breathing propulsion, this is the desired condition for cruise. The second category is the trim glide condition, with flight-path angle and velocity appropriate to quasi-steady flight at $L/D_{max}$. The third category is represented by a single case, a maximum range trajectory to a trim glide condition at an altitude of 45,000 ft. Terminal altitudes considered for the first 2 categories are 45,000–150,000 ft.

The terminal velocity and flight-path angle for a given altitude must be found iteratively, as the lift and drag coefficients, $C_L$ and $C_D$, are functions of $M$ as well as $\alpha$.

The terminal conditions are plotted against altitude in Fig. 1.

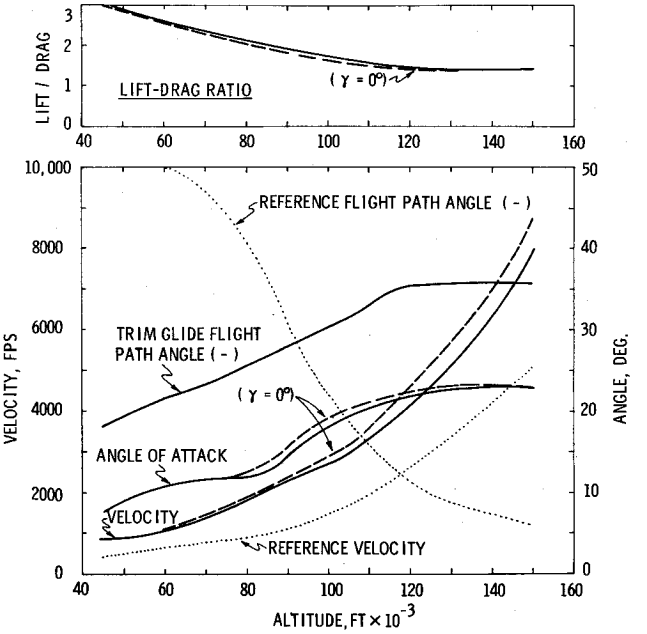


**Fig. 1 Equilibrium flight conditions ($\gamma = 0$) for straight-wing orbiter at maximum lift-drag ratio.**

The trim flight-path angle, $\gamma$, ranges between $-18.1°$ and $-35.8°$, as $L/D$ drops from 3.1 to 1.4, and the velocity rises from 839 to 7993 fps ($M = 0.87$–$7.45$). The relatively high zero-lift drag at transonic speeds and above causes the maximum lift-drag ratio to occur at angles of attack between 7.3° and 22.9°. For zero $\gamma$, increased lift is required to counteract gravity; hence, the velocity is increased, and there is a small change in $\alpha$ and $L/D_{max}$.

The velocity and $\gamma$ from a constant-$\alpha$ trajectory ($\alpha = 60°$) also are shown in Fig. 1. In all cases, the equilibrium flight condition requires increased velocity at a given altitude. A pullup is required to meet all horizontal equilibria and trim glide equilibria below 92,000 ft, while $\gamma$ is forced to become steeper for trim glide conditions above 92,000 ft.

### Minimal Load Factor Trajectories

Transition maneuvers which meet the end conditions while minimizing the load factor's deviation from 1 $g$ are demonstrated in this section. No penalty for flight in an intermediate $\alpha$-region is imposed, i.e., the $k_3$ of Eq. (10) is zero. Quadratic penalties are levied for $\alpha$ greater than 60° or less than 3°. The trajectories discussed here minimize load factor error only locally. The maximal range trajectory discussed in a later section yields lower load factor cost; however, this trajectory could not be obtained by using the corresponding high-$\alpha$ profile of this section as an initial control profile, and it is assumed to be a trajectory of a different class. In addition to locally minimum load factor, the trajectories of this section are characterized by low dynamic pressure. Trajectories to terminal altitudes of 75,000 ft or less are further characterized by low heat load.

Control and flight parameter profiles for the transition to trim glide are shown in Figs. 2 and 3. The greatest similarity in these trajectories is that the large $\alpha$-maneuver is relatively abrupt, and it occurs at nearly the same flight time in all cases (Fig. 2a). The $\alpha$-profiles show greater spread when plotted against altitude (Fig. 2b). Figure 2 also indicates that negative $\alpha$ is required to provide the steep flight-path angles associated with trim glide at high terminal altitude. Figure 3 shows that higher Mach number and shallow $\gamma$ are encountered in the early phase of the transition to high altitude, the result of reducing $C_D$

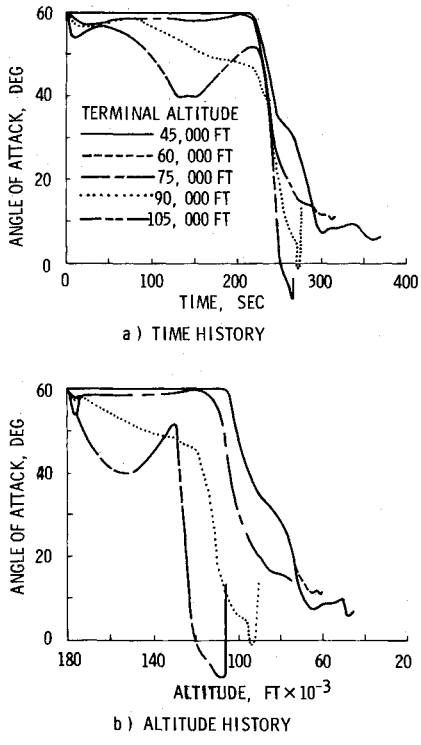


**Fig. 2 Optimal angle-of-attack profiles for trim glide terminal flight-path angle.**

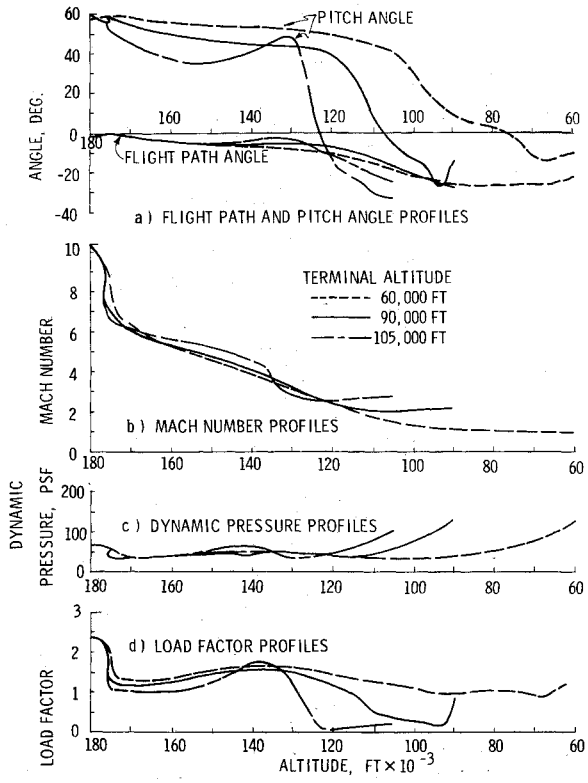


**Fig. 3 Parameters of the transition with trim glide terminal flight-path angle.**

and operating in the region of $C_{L_{max}}$ prior to the pitchdown. The trajectories terminating in the trim-glide condition have moderate dynamic pressure profiles and low load factor, with the 105,000-ft case experiencing a free fall near its end point. In all cases the terminal dynamic pressure is the maximum value on the profile.

Transitions to zero $\gamma$ at altitudes up to 150,000 ft present no particular dynamic problem, although there is an increase in heat load commensurate with higher mean velocity. Figure 4 shows

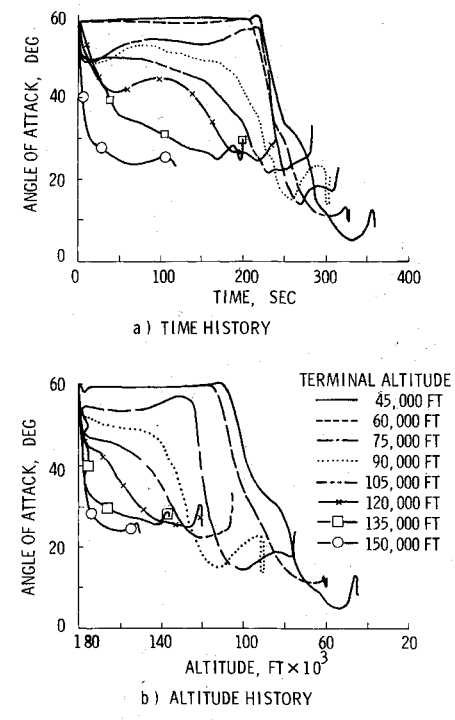


**Fig. 4 Optimal angle-of-attack profiles for zero terminal flight-path angle.**

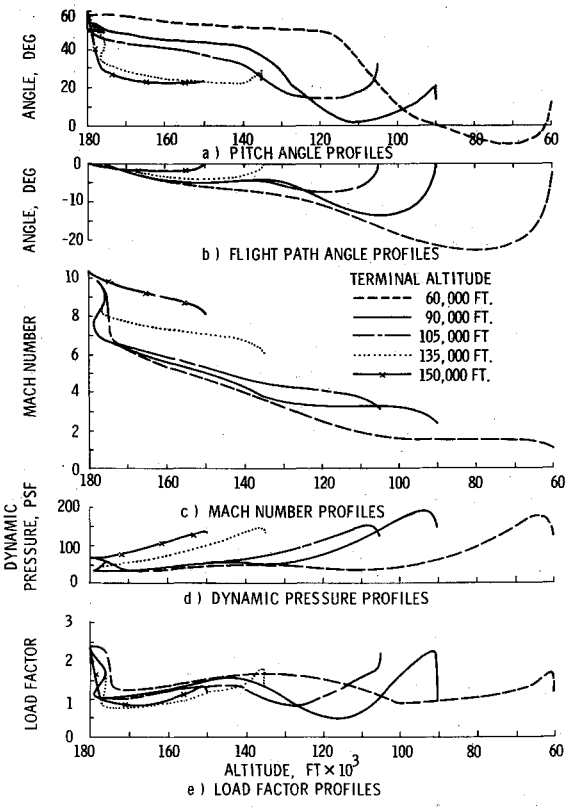


**Fig. 5 Parameters of the transition with zero terminal flight-path angle.**

time and altitude histories for 8 zero $\gamma$ cases. For terminal altitudes of 45,000–60,000 ft, excess energy is dissipated as in the trim glide cases, and a single large $\alpha$-change occurs late in the transition. For terminal altitudes between 75,000 and 120,000 ft, there are 2 significant $\alpha$ maneuvers, the first primarily affecting altitude and velocity and the second adjusting $\gamma$. Figure 5 indicates that for all cases in the first 2 classes there is a knee

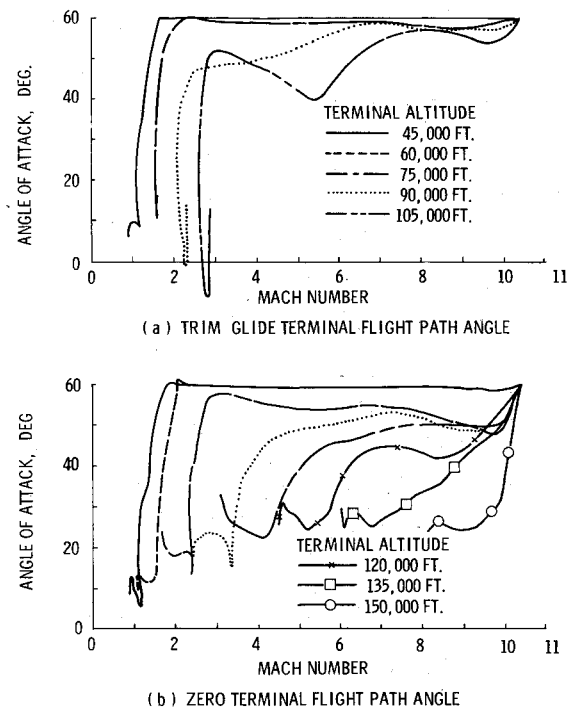


**Fig. 6 Angle of attack vs mach number for optimal straight-wing orbiter transitions without intermediate penalty.**

in the $\gamma$ curve at approximately 130,000 ft. The third class of transition is illustrated by the remaining 2 cases, which have a single $\alpha$ transition beginning immediately. The 135,000- and 150,000-ft cases are typified by early transition to the maximum lift-drag ratio, which results in reduced energy dissipation and negligible change in flight-path angle. In all 8 cases, Mach number decreases monotonically, and dynamic pressure peaks during the transition exceed the terminal values. The optimization process is particularly sensitive to terminal $\gamma$ errors, causing large control angle excursions in the last few seconds of these runs. Heating is 3%–25% higher for the zero $\gamma$ terminal conditions than for the trim glide terminal conditions, while ground range is 2%–21% greater.

Figure 6 presents $\alpha$ as a function of $M$ for the cases discussed in this section. The most striking feature of these curves is that, in 8 of the 13 cases, the large $\alpha$ maneuver occurs at nearly constant Mach number.

### Stability-and-Control Boundaries

The minimal load factor trajectories do not take into account the orbiter's pitching moment characteristics. Although the angle-of-attack profiles produce the desired flight paths, there is the possibility that the longitudinal control moment is incapable of trimming the spacecraft at the intended operating point or that a reachable point is unstable; thus, the static moment characteristics of the vehicle define satisfactory, unsatisfactory, and unreachable regions in the trajectory space. Reshaping the trajectory to avoid the unstable or unreachable regions reduces control requirements and increases the margin of safety and reliability.

The principal condition of static longitudinal stability at a fixed or slowly changing flight condition is that the aerodynamic pitching moment counteracts $\alpha$ perturbations. This occurs when the $\alpha$-derivative of the moment coefficient, $C_m$, is locally less than zero.

$C_m$ vs $\alpha$ curves which are typical of straight-wing and delta-wing orbiter characteristics are plotted in Fig. 7. Stable equilibrium points are readily identified by abscissa crossings with negative slope, while unstable equilibria have crossings with

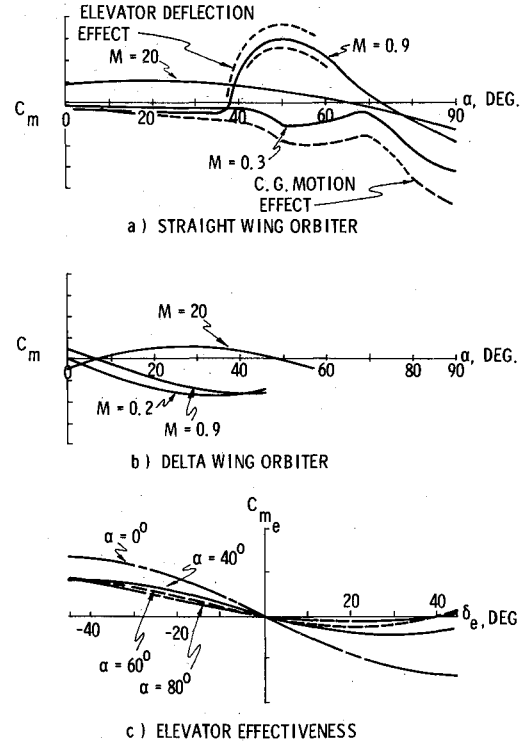


**Fig. 7 Pitching moment and longitudinal control moment coefficients.**

positive slope. The basic effect of elevator deflection, $\delta$, is to translate the $C_m$ vs $\alpha$ curves up and down, while c.g. movement primarily rotates the curves about a point near $\alpha = 0°$; thus, $\delta$ causes the equilibrium point to vary, while c.g. location affects both the angle for equilibrium and the stability of the equilibrium. The effect of Mach number is more complex, as fundamental changes in the flow about the body and the resulting pressure distribution occur.

Figure 7 indicates that the pitchup instability, which occurs when $\partial C_m/\partial\alpha$ becomes positive, is present at subsonic and transonic speeds for both the straight-wing and delta-wing configurations; however, it is especially severe for the straight-wing orbiter in transonic flight. An elevator with adequate control authority for subsonic flight is unable to produce an equilibrium at $\alpha = 50°$: the required moment increment is too great. In hypersonic flight, both configurations have similar moment curves, exhibiting stability at high angle and instability at low angle.

Although the pitching moment is usually assumed to be a linear function of control surface deflection, this approximation is invalid for large surface deflections and at high angles of attack. Experimental data collected by Decker and Spencer[12] show that low-$\alpha$ control moment is relatively symmetric in $\delta$; it is linear for $-20° < \delta < 20°$ and reaches maxima and minima for $\delta = \pm 40°$. At high angles of attack, the control effect becomes asymmetric, and control reversal occurs for $\alpha$ above 60° ($\delta > 30°$, $\delta < -40°$). Positive elevator deflection (trailing edge down) is sufficiently weak at high $\alpha$ that other experimenters have published data for negative deflection alone.[13,14]

It has been found that Newtonian Theory provides a remarkably good estimate of elevator effectiveness at high angle of attack ($\alpha \geq 40°$) for both subsonic and hypersonic Mach number. The good subsonic agreement is probably due to the separated, blunt body flow and the lack of wing interference on the tail at high $\alpha$.

Assuming that the vertical displacement of the elevator's aerodynamic center can be neglected, the control moment coefficient predicted by Newtonian Theory is

$$\Delta C_{m_e} = (2\, l_e S_e/\bar{c}S)\, \sin^2(\alpha + \delta) \cos\delta \qquad \alpha \gg 0 \qquad (12)$$

where $l_e$ and $S_e$ are the elevator's distance from the c.g. and its surface area. Control reversal then occurs when

$$\tan(\alpha + \delta) = 2 \cot\delta \qquad (13)$$

Equation (13) indicates that control reversal will occur at lower deflections as $\alpha$ is increased.

Elevator-effectiveness curves representative of straight-wing orbiter wind-tunnel data are illustrated in Fig. 7c at a scale which is roughly double that of Fig. 7a and b (and which is also dependent on $M$). The moment available for control is seen to decrease with increasing $\alpha$, and the high-$\alpha$ asymmetry is apparent. There is an overall magnitude reduction at transonic speed which, combined with the pitchup characteristic, greatly reduces the flexibility of control near $M = 1$.

Longitudinal control boundaries for a straight-wing orbiter are presented in Fig. 8. Solid lines indicate boundaries confirmed by wind-tunnel testing, while dashed-line boundaries are estimated. Areas marked as "Control Authority Exceeded" indicate $\alpha$-$M$ combinations for which $C_m$ cannot be brought to zero by elevator deflection. These areas could be penetrated in dynamic maneuvers or by using reaction control thrusters, but the spacecraft cannot be trimmed in these areas by the elevator alone. "Unstable" marks areas of positive $\partial C_m/\partial\alpha$. Figure 8 illustrates why the original plans for subsonic transition ran into difficulty. By maintaining high $\alpha$ to low Mach number, the $\alpha$ vs $M$ profile is squeezed into a narrow region between control boundaries, and this region is very sensitive to c.g. location. Aft movement of the center of gravity raises the upper and lower control boundaries, broadening the unstable band as well. If elevator deflection is restricted, the aft c.g. also will

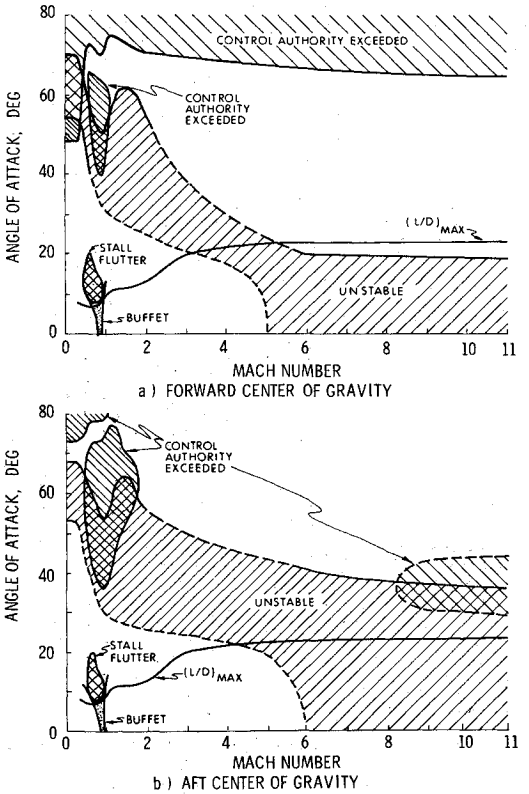


**Fig. 8 Straight-wing orbiter control boundaries.**

introduce an unreachable region along the boundary of instability at hypersonic $M$.

The $\alpha$ vs $M$ profile for maximum lift-drag ratio is included in Fig. 8. This profile constitutes a preferred path from the standpoint of maximum maneuverability. A forward location puts the $L/D_{max}$ curve in a stable control region at hypersonic $M$; an aft location imbeds the curve in an unstable region and may render it unreachable.

For comparison, the control boundaries of a delta-wing orbiter are shown in Fig. 9. The most obvious change from Fig. 8 is the

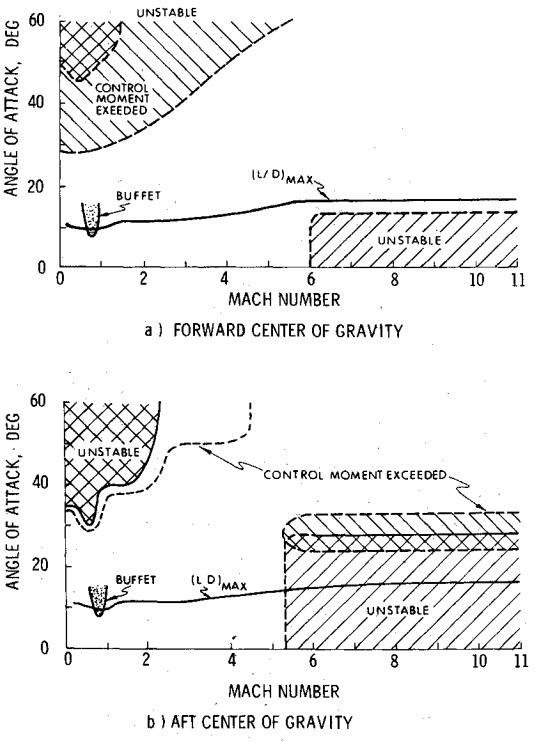


**Fig. 9 Delta-wing orbiter control boundaries.**

absence of an unstable band separating the entry and terminal regions. The pitchup instability exists for $M < 2$, and the hypersonic low-$\alpha$ instability is present. Control authority boundaries are again dependent on elevator (or elevon) size and moment arm as well as c.g. location. Aft movement of the c.g. raises the upper control moment boundary to higher $\alpha$ but causes the pitchup instability boundary to occur at lower $\alpha$. The c.g. location effect on the attainability of $L/D_{max}$ is similar to that of the straight-wing orbiter, although the problem could be of more concern for the delta-wing configuration, which might be expected to fly at $L/D_{max}$ at a higher $M$. Furthermore, $L/D_{max}$ occurs at a lower angle of attack than for the straight-wing orbiter.

### Trajectories with Angle Constraints

When the internal $\alpha$-penalty of Eq. (11) is imposed, the optimal angle-of-attack profiles are modified to spend less time in the penalty region. The abrupt change in $\alpha$ perturbs the spacecraft's phugoid mode (the long-period, oscillating interchange of potential and kinetic energy) causing peaks in dynamic pressure, Mach number, and load factor following the jump. These peaks are minimized and the terminal state is obtained by optimal reshaping of the $\alpha$-profile before and after the jump. Previous studies for an $\alpha$-penalty which is independent of $M$ show that $\alpha$ approximates the minimal load factor profile until the upper penalty boundary is reached; $\alpha$ stays on the boundary until the $\alpha$ for minimal $g$ approaches the mid-point of the penalty region.[5] The angle jumps at a rate controlled by the penalty weight, then follows the lower boundary until the minimal $g$ profile is encountered. Similar results occur when $\alpha$ is a function of $M$.

Figure 10 shows $\alpha$ vs $M$ for constrained trajectories to various terminal altitudes with forward and aft center of gravity locations. With forward c.g., satisfactory equilibria can be obtained for all cases except the 105,000-ft and 120,000-ft terminal conditions, which lie in the unstable region. With aft c.g., terminal altitudes above 120,000 ft must be excluded by the same criterion.

Time histories of angle of attack and flight variables are presented in Fig. 11. The figure shows that $\alpha$ does jump rapidly from high to low angle, and the dynamic pressure and $M$ rise above the minimal load factor values. The maximum increase in post-jump $M$ is 0.2, a matter for little concern. Additional data are tabulated below.

Unlike the subsonic transition results,[5] no substantial increase in dynamic pressure, load factor, or dive angle is caused by the jump maneuver. Figure 11 shows that dynamic pressure rises above minimal q values following the jump; however, peak values are nearly the same for all 3 cases. Maximum load factors are associated with the terminal pullup rather than the transition jump; hence (with the exception of the 60,000-ft aft c.g. case) the $\alpha$ maneuver changes these values little. The reason for these results is indicated by the third parameter in Table I, pitch angle ($\theta$). The supersonic transition jump occurs at a shallow flight path angle, ranging from $-22°$ to $-4°$, while the subsonic transition jump $\gamma$ is $-40°$ to $-45°$. In the latter case, the maximum negative $\theta$ occurs immediately following the jump; in the former case, $\theta$ remains positive for some time after the jump, and the maneuver does not induce a dive. The maximum negative $\theta$ occurs near the final time.

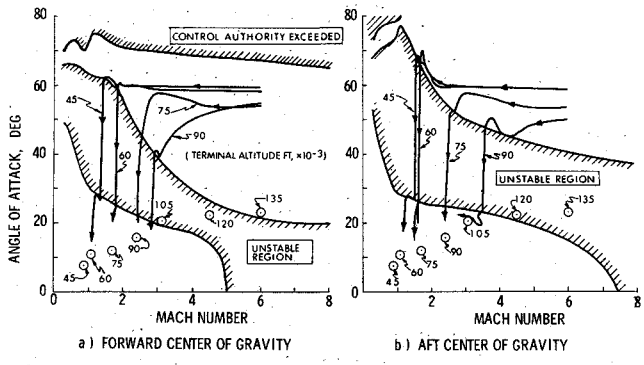


**Fig. 10 Angle-of-attack profiles for constrained transition trajectories.**

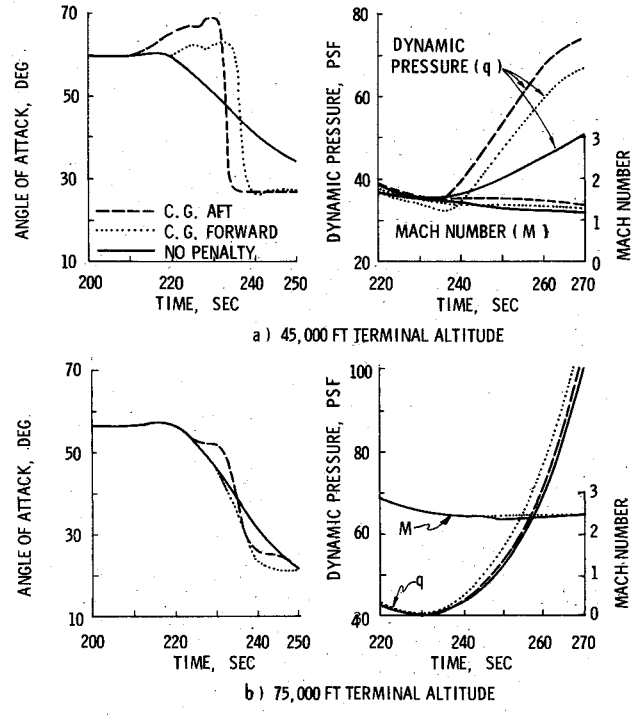


**Fig. 11 Flight parameters for the jump transition.**

### Gliding Trajectories between High- and Low-Altitude Equilibrium Conditions

It has been shown that zero $\gamma$ equilibrium flight conditions can be obtained at altitudes up to 150,000 ft. While these conditions have been considered final, there is the need to maneuver to a position at lower altitude, e.g., a high key point for landing

**Table 1 Extreme value of flight variables following transition jump**

| Altitude, ft | Dynamic pressure, psf | | | Load factor | | | Pitch angle, deg | | |
|---|---|---|---|---|---|---|---|---|---|
| | Min g | Aft c.g. | For c.g. | Min g | Aft c.g. | For c.g. | Min g | Aft c.g. | For c.g. |
| 45,000 | 234 | 235 | 222 | 1.9 | 2.0 | 1.9 | −20.2 | −21.6 | −20.0 |
| 60,000 | 175 | 183 | 181 | 1.6 | 2.1 | 1.5 | −9.0 | −14.3 | −6.0 |
| 75,000 | 197 | 199 | 198 | 2.3 | 2.4 | 2.3 | −5.9 | −5.7 | −5.5 |
| 90,000 | 188 | 194 | 193 | 2.2 | 2.1 | 2.0 | +2.0 | +3.8 | 3.4 |

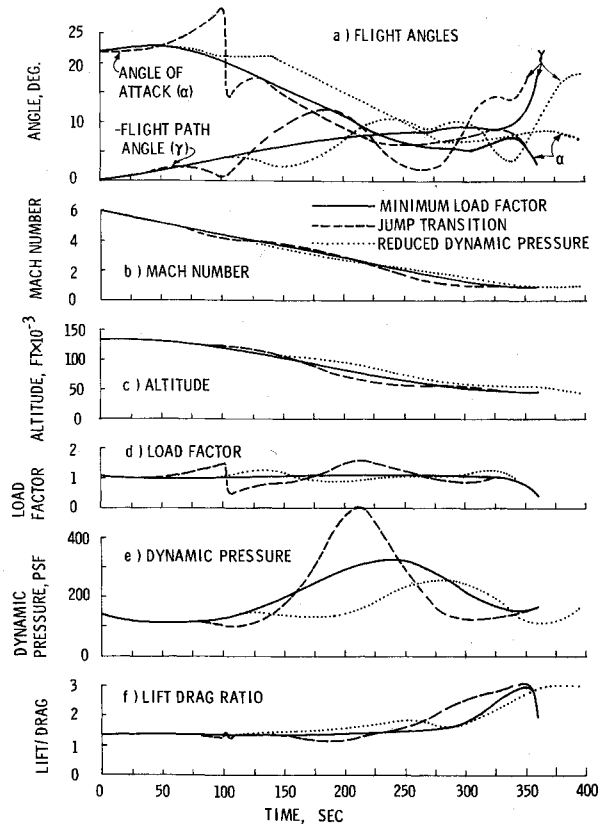


**Fig. 12 Flight parameters for gliding trajectories from 135,000 ft-to 45,000 ft-altitude.**

approach. This segment of the flight back from orbit can be characterized as a glide at moderate-to-low $\alpha$, although the spacecraft may not be in an equilibrium glide until the end of the segment.

A 135,000-ft zero $\gamma$ condition has been chosen as a starting point for the gliding trajectories to follow. This flight condition lies above the straight-wing orbiter's unstable region (for forward c.g.), and transitions to higher-altitude equilibrium conditions can be expected to pass near this point (defined by $\alpha$, $M$, $\gamma$, and altitude) on their gliding trajectories. A 45,000-ft equilibrium glide defines the gliding trajectory end point.

Figure 12 shows that the minimum load factor path from the Mach 6 starting point to the subsonic end point is smooth, with gradual decrease in $\alpha$ and a nearly linear reduction in $M$. Flight-path angle steepens in the 20 sec prior to reaching 45,000 ft, as the spacecraft dives to the condition for equilibrium glide. Pitch angle, which is indicated by the difference in the $\alpha$ and $-\gamma$ curves [since $\theta = \alpha - (-\gamma)$], is positive for the first 225 sec and negative for the remainder of the flight. Lift-drag ratio is generally near $L/D_{max}$ for $M > 4$ and is less thereafter, approaching $L/D_{max}$ again at the dynamic pressure minimum prior to the terminal point. With the exception of the terminal dive, load factor is near 1 throughout the flight.

Figure 12 shows a gliding trajectory which minimizes the first problem by employing a jump transition through the unstable region. For the forward c.g. position, the initial $\alpha$ lies in a stable region; however, as $M$ decreases, $\alpha$ must increase to avoid the unstable region shown in Fig. 8(a). After the jump, through which $\theta$ remains positive, $\alpha$ follows the lower penalty boundary, then varies to meet the terminal conditions. The $\alpha$ jump perturbs the phugoid mode, causing an oscillatory $\gamma$, a maximum load factor of 1.6, and a maximum $q$ of 500 psf.

The dynamic pressure peaks for these 2 cases may be excessive; a solution can be found by minimizing dynamic pressure rather than load factor or $\alpha$ penalty. The third trajectory shown in Fig. 12 indicates that the dynamic pressure peak can be reduced by flying at higher altitude (by increasing $L/D$). This result is obtained at the expense of load factor variation which is, nevertheless, not large.

### Maximal Range Trajectories

In all of the previous cases, the terminal state cost has been independent of range, i.e., $q_{44} = 0$ in Eq. (8). If a linear terminal cost of the form

$$\psi = rx_4 \qquad r < 0 \tag{14}$$

is included in the optimization, range will be maximized subject to the other terminal and integral costs. Equation (14) produced such a powerful effect in reducing angle of attack at zero time that Eq. (11) was consistently violated, i.e., it was impossible to maintain an initial $\alpha$ near 60°. To overcome this, $\alpha$ was reduced from 60° to 30° at 3°/sec for the first 10 sec, and the optimization proceeded from this point on. For the trajectories which follow, the 45,000-ft trim glide establishes the terminal flight condition.

Figure 13 compares the maximal range trajectory to 45,000-ft altitude with the corresponding low $L/D$ (or high-$\alpha$) minimal load trajectory to the same terminal condition. Elapsed range increases from 239 naut miles to 522 naut miles as a consequence of the higher mean velocity and increased flight time of the maximal range trajectory. This condition is maintained by an $L/D$ near maximum value throughout most of the flight. The 118% increase in range causes the increased heat load (5887 vs 1591 Btu/ft$^2$) and maximum $q$ (314 vs 187 psf); however, load factor is sharply reduced.

As suggested earlier, intermediate $\alpha$ constraints are cause for more concern with an aft c.g. location than with a forward center of gravity. In the latter case, range is unaffected by the transition jump. In the former case, however, $\alpha$ is constrained to the upper penalty boundary prior to the transition jump, reducing hypersonic $L/D$ and decreasing range by more than 80 naut miles.

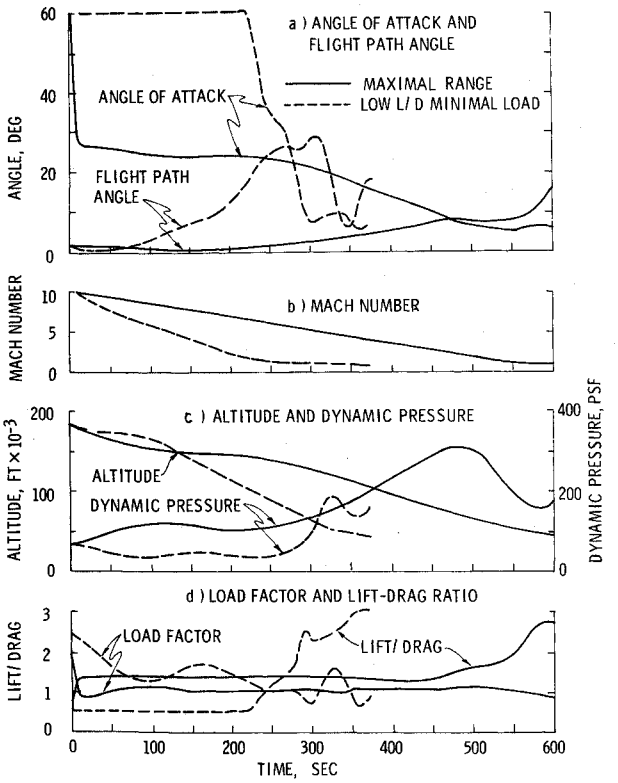


**Fig. 13 Flight parameters maximal range and minimal load trajectories which terminate at 45,000 ft-altitude.**

## Conclusions

Subjecting the control to terminal state and integral load factor penalties alone, it is found that there are at least 2 locally minimizing paths to low-altitude end conditions. The first trajectory class is characterized by high $\alpha$ during the early portion of flight, low-heat load, and low-dynamic pressure. The second trajectory class exhibits a rapid pitch-down to an $\alpha$ which yields maximum lift-drag ratio. Load factor cost is less for this class, and range is significantly increased, but the increased mean velocity leads to higher heat load and maximum dynamic pressure. For terminal conditions at high altitude, only the second class occurs.

Because $L/D_{max}$ is low at transonic and supersonic speeds, trim-glide flight-path angles are very steep at the terminal conditions. While it is possible to establish a trim glide for altitudes up to at least 105,000 ft, negative $\alpha$ is required to meet the higher altitude flight conditions. It is possible, however, to obtain horizontal flight, with $\dot{\gamma} = 0$ and load factor near 1, at higher altitudes. The latter strategy conserves horizontal maneuverability and does not require negative $\alpha$. The end point of such a transition can be matched to a trim-glide high key point at lower altitude with a low-$\alpha$ gliding trajectory.

Flight duration through imbedded regions of instability can be minimized by using an abrupt jump in angle of attack. It is found that this jump is more easily made at supersonic speed than at sub- or transonic speed. Not only is the transonic unstable region especially broad, it also contains an unreachable region, i.e., a region in which control authority is insufficient to null the pitching moment. Furthermore, high Mach number transitions occur at more shallow flight-path angles than subsonic transitions; hence, they do not require steep dive angles nor do they cause substantial increases in $M$, maximum $q$, or maximum load factor.

The location of stability-and-control boundaries, both interior and exterior, depends of the spacecraft's c.g. location. Forward c.g. lowers the $\alpha$ boundaries, a generally favorable result, since $L/D_{max}$ occurs at a relatively low angle. Aft c.g. movement enlarges the imbedded region for the prototype spacecraft. In addition, aft c.g. may cause unreachable regions to occur at moderate $\alpha$ and high $M$.

## References

[1] "Shuttle Performance Gain Planned," *Aviation Week and Space Technology*, Vol. 94, No. 6, Feb. 8, 1971, p. 16.

[2] Faget, M., "Space Shuttle: A New Configuration," *Astronautics and Aeronautics*, Vol. 8, No. 1, Jan. 1970, pp. 52–61.

[3] Draper, A., Buck, M., and Goesch, W., "A Delta Shuttle Orbiter," *Astronautics and Aeronautics*, Vol. 9, No. 1, Jan. 1971, pp. 26–35.

[4] "A Concept of a Manned Satellite Reentry Which is Completed with a Glide Landing," TM X-226, Dec. 1959, NASA.

[5] Stengel, R., "Optimal Transition from Entry to Cruising Flight," *Journal of Spacecraft and Rockets*, Vol. 8, No. 11, Nov. 1971, pp. 1126–1132.

[6] Stengel, R., "Space Shuttle Transition to Cruising Flight," Rept. E-2539, Sept. 1970, MIT Charles Stark Draper Lab., Cambridge, Mass.

[7] Bryson, A. E. Jr. and Ho, Y., *Applied Optimal Control*, Blaisdell, Waltham, Mass. 1969.

[8] Lasdon, L., Mitter, S., and Waren, A., "The Conjugate Gradient Method for Optimal Control Problems," *IEEE Transactions on Automatic Control*, Vol. AC-12, No. 2, April 1967, pp. 132–138.

[9] Mehra, R. K. and Bryson, A. E., Jr., "Conjugate Gradient Methods with an Application to V/STOL FLIGHT Path Optimization," *Journal of Aircraft*, Vol. 6, No. 2, March-April 1969, pp. 123–128.

[10] Pu, C. L., "Numerical Solution of Dynamic Optimization Problems," Rept. E-2549, Feb. 1971, MIT Charles Stark Draper Lab., Cambridge, Mass.

[11] *MSC Space Shuttle Aerodynamic Design Data Book, Vol. 1—Orbiter Aerodynamic Design Data*, July 1970, NASA, Rev. Aug. 1970.

[12] Decker, J. and Spencer, B. Jr., "Low-Subsonic Aerodynamic Characteristics of a Model of a Fixed-Wing Space Shuttle Concept at Angles of Attack to 76°," TM X-1996, April 1970, NASA.

[13] Stone, D., "Aerodynamic Characteristics of a Fixed-Wing Manned Space Shuttle Concept at a Mach Number of 6.0," TM X-2049, Sept. 1970, NASA.

[14] Freeman, D., Jr., "Low-Subsonic Aerodynamic Characteristics of a Space Shuttle-Orbiter Concept with a Blended Delta Wing-Body," TM X-2209, Jan. 1971, NASA.